Negative Hydrogen Ion Transport in RF-driven Ion Sources for ITER NBI

R. Gutser, D. Wünderlich, U. Fantz and the NNBI-Team

Max-Planck-Institut für Plasmaphysik, Euratom Association, D-85748 Garching, Germany

E-mail: raphael.gutser@ipp.mpg.de

Abstract. The injection of energetic neutral atoms is a major component of plasma heating in fusion experiments. In order to fulfill the requirements of the ITER neutral beam injection (NBI), a RF-driven ion source for negative ions has been developed at the MPI für Plasma Physik (IPP Garching). Negative hydrogen ions are generated on a converter surface by impinging neutral particles and positive ions under the influence of magnetic fields and the plasma sheath potential. A 3D negative ion trajectory calculation including a Monte Carlo description of reactions and collisions with plasma particles was used to calculate the total and spatially resolved extraction probabilities for realistic field topologies and geometries of the large scale extraction system LAG. The experimentally observed increase of extracted ion current by the use of chamfered aperture collars agrees with results of the ion transport simulation. Profiles of the extraction probability on the converter show that most of the extracted negative ions are created in the vicinity of the plasma grid apertures. These areas of intensified extraction probability are influenced by the magnetic field configuration. The ion extraction probability is affected by the long ranging magnetic filter field. The short ranging electron deflection field however, which is generated by magnets near the converter surface, does not significantly influence the extraction probability.

1. Introduction

Next generation fusion experiments such as ITER will use high performance neutral beam injection (NBI) systems for heating and current drive. While the neutralization efficiency for systems based on positive hydrogen ions tends to zero for energies above 200 keV, the neutralization efficiency of negative hydrogen ions is still 60% for the required energy of 1 MeV D [1]. The low binding energy (0.75 eV) of the addition electron, which is beneficial to neutralization, causes short survival lengths inside the plasma of the ion source. Thus, the current densities delivered by negative ion sources are typically a factor of ten lower compared to positive ion sources.

The ion source used for ITER must deliver 40 A of D^- ions for 3600 seconds at a source pressure of 0.3 Pa while maintaining an electron to ion ratio < 1 [2] [3]. At negative ion current densities of $j_{D^-} = 200\text{-}300$ A/m^2, the effective extraction area will be 2000 cm^2. The RF-driven ion source, developed at the MPI für Plasma Physik fulfils the physical

aspects of these requirements [4]. In addition, the basically maintenance-free operation of the ion source is beneficial to fulfill the remote handling requirement of ITER. As a consequence of this development, ITER has decided to adopt the RF-driven ion source as the reference source for the neutral beam injectors [2].
The ion current delivered by negative ion sources is considerably low compared to the ion current extracted from positive ion sources. Understanding of the negative ion extraction process is essential to optimize the source efficiency, but is still an open issue [5]. Numerical models can help to enhance the understanding of the physical processes within the negative ion source in order to optimize the performance and to predict the results of parameter changes. Promising approaches to model the negative ion extraction are probabilistic ion transport codes [6] [7]. However, the existing codes use in several aspects simplified assumption regarding the converter geometry and the configuration of the magnetic and electric fields. Hence, the TrajAn (Trajectory Analysis) code was developed to consider these physical aspects.
The complex nature of the large-scaled magnetic field topologies and converter geometries in the RF-driven ion source demands the use of realistic field and geometry models. The modeling of complex 3D magnetic and electric fields by external codes makes it possible to perform simulations of the complete converter system. An exact geometric model of the converter geometry allows a more detailed consideration of the starting conditions of the negative ions, which play a very important part in the physics of ion transport. Furthermore, the code is capable to calculate profiles of the extraction probabilities on the converter surface and of the current density distribution over the extraction apertures. This spatial resolution makes it possible to detect areas of intensified ion production on the converter and to resolve the current density distribution in individual beamlets. This is especially important for beam optics calculations, where the current density distribution is used as an input parameter.
A brief description of the RF-driven ion source is given in the following section, while detailed information regarding the individual components and operation parameters are available from [4].

2. The RF-driven Negative Ion Source

Figure 1 gives a schematic overview of the ion source, which is divided into three parts: driver, expansion region and extraction region. In the chosen coordinate system, the x-axis is aligned in beam direction, while the z-axis points in the direction of the magnetic filter field lines. A low pressure and low temperature plasma is generated by 1 MHz RF coils at a pressure of 0.3 Pa inside the driver. A maximum RF generator power of 120 kW is available per coil. The plasma enters the expansion region where a magnetic filter is generated by permanent magnets at the source periphery. This field is necessary to keep "hot" electrons (T_e >2 eV) away from the regions, where negative ions are generated, in order to avoid collisional destruction.
The dominant generation mechanism for negative ions is the surface effect: positive

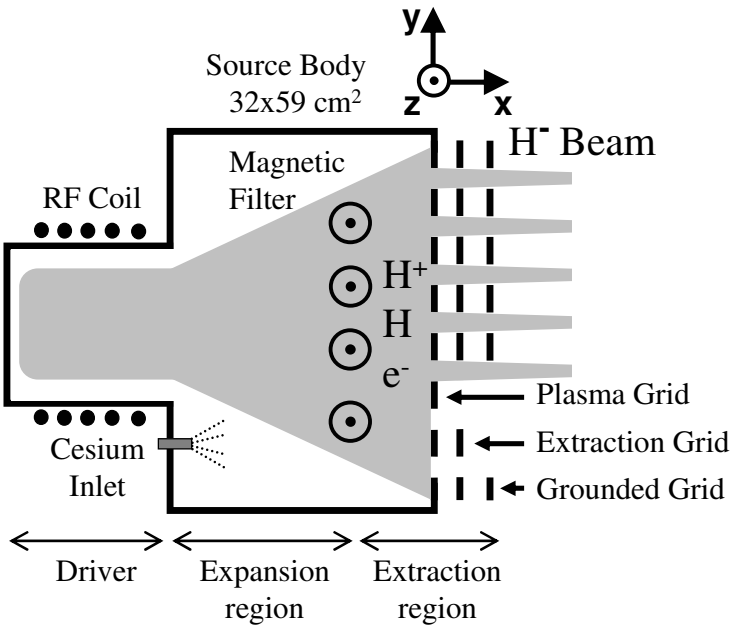

Figure 1. Schematic view of the IPP RF-driven ion source showing driver, expansion and extraction region including the three grid extraction system.

or neutral hydrogen plasma particles are converted into negative ions by picking up electrons from a converter surface. In the RF-driven ion source, the plasma grid (see figure 1) is used as converter for the surface generation process. Measurements [8] show typical plasma parameters of T_e=2 eV electron temperature and n_e=$5 \cdot 10^{17}$ m^{-3} electron density in front of the plasma grid. The path length of surface generated negative ions is limited by collisions with the background plasma. Typical path lengths of several centimeters (see section 5.1) arise at the plasma parameters of the RF-driven ion source. As a consequence, only negative ions generated on the plasma grid surface are able to contribute to the extracted current density. In order to increase the conversion rate, a cesium coating is used to lower the work function [9] of the plasma grid surface. This is achieved by evaporating elemental cesium from a liquid cesium reservoir into the ion source. The surface generated negative ions are accelerated back into the plasma volume by the plasma sheath potential and have to bent back by collisions and the magnetic field in order to be extracted. This sheath potential can be influenced by biasing the plasma grid against the source body.

The negative ions entering the extraction system through the plasma grid apertures are immediately accelerated by the extraction voltage. The ion beam formation is accomplished in two stages by a three grid system: the plasma grid, the extraction grid and the grounded grid. In the first step, a voltage of $8 - 10$ kV is applied between the plasma and the extraction grid in order to allow the removal of co-extracted electrons at

reasonable energies. A second voltage of $20 - 30$ kV is used for acceleration at the test facility of the IPP. Electron removal is done by a mass selective magnetic field. This electron deflection field is generated by CoSm magnet rods inside the extraction grid. A detailed analysis of the magnetic field structure of the IPP RF-driven ion source is presented in the following section.

3. Magnetic Field Configuration

The 3D magnetic topology results from a superposition of two fields components:

(i) filter field

(ii) deflection field

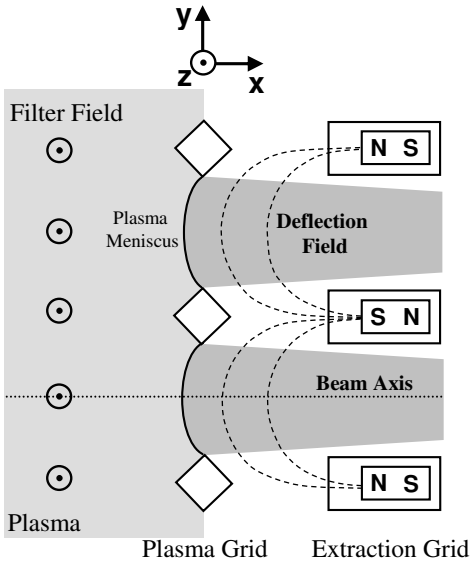

Figure 2. Magnetic field structure at the the extraction region.

Figure 2 gives an overview of the magnetic fields at the extraction region. The filter field is generated by boxes of aligned permanent magnets attached to the walls of the source body. By this means, a directed field in positive z-direction is generated between the magnets. Figure 3(a) shows a contour plot of the filter field component $B_{\mathrm{z}}^{\mathrm{Filter}}$ in the zy-plane at the position of the plasma grid (x=0) including the extraction apertures of the plasma grid. Owing to the proximity to the magnet boxes, the field intensifies at the edges of the extraction system. The asymmetric field structure is a consequence of the arrangement of the magnet boxes.

While the filter field is present in the whole extraction region, the electron deflection field is localized near the plasma grid. The deflection field is generated by permanent magnet rods with alternating magnetization inside the extraction grid as shown in figure 2. Therefore, the direction of the deflection field alternates along the aperture

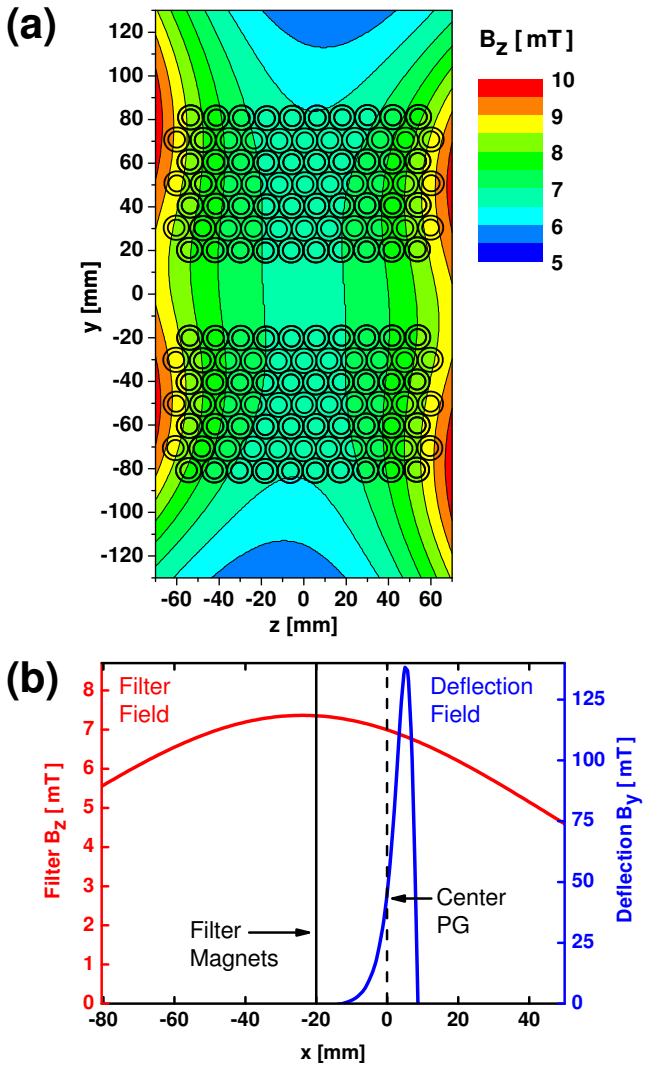

Figure 3. (a) Contour plot of the B_z^{Filter} component of the magnetic filter field at the position of the plasma grid apertures. (b) Profiles of the filter and electron deflection field in x-direction through a beam axis. The sign of the deflection field depends on the individual magnet row. **Dashed Line**: position of the plasma grid apertures. **Solid Line**: position of the permanent magnet boxes for the filter field.

rows and the field lines are perpendicular to the field lines of the filter field. Figure 3(b) shows the variation of the main filter and deflection field components in x-direction. The calculation is done for a line at the center of an extraction aperture (beam axis in figure 2). The filter field has a Gaussian shaped profile with a peak strength of 7 mT at the position of the magnet boxes at x=-20 mm. In contrast, the deflection field reaches its maximum strength at the position of the extraction grid for x=10 mm. Nevertheless, the field penetration into the plasma is limited owing to the alternating magnetization of the magnet rods. Hence, the deflection field is localized near the plasma grid. In

summary, the magnetic field configuration consists of the weak, but long ranging filter field and a strong, but localized deflection field.
A description of the numerical model and the input parameters is given in the following section.

4. Monte Carlo Transport Simulation

4.1. Simulation Overview

In order to describe the negative ion transport from the converter to the extraction region, the three dimensional equation of motion within the magnetic and electric field topology of the ion source is solved. Elastic and inelastic collisions of negative ions with plasma particles are simulated using Monte Carlo methods. The complex magnetic field topology was calculated by the Finite Element method. No strong electrical fields occur in the plasma volume. Although magnetized electrons generate electrical fields perpendicular to the alignment of the magnetic field lines, this effect is compensated by the influence of high electron mobility on the magnetic field lines between the unipotential wall surfaces resulting in a very low gradient of T_e.
Electrical fields in the plasma sheath, which result in an initial acceleration of negative ions into the plasma, are very important for the transport investigation. Because of the small extension of the plasma sheath related to the extension of the total computation domain, effects of the plasma sheath were implemented by a finite starting energy of the surface generated negative ions. This energy is used as an input parameter for the transport studies. The converter surface geometry was accurately modeled according to the experimental conditions including chamfered edges [4] and arrangement of the individual apertures. A detailed view of the plasma grid geometry is given by figure 5.
Because of the non-zero initial velocity prior to acceleration in the plasma sheath, the initial direction of the negative ions perpendicular to the converter surface is broadened according to a cosine distribution [10].
The angular distribution and absolute value of the initial velocity vector used in the transport code represent the initial energy of the ions at the surface and the acceleration within the plasma sheath. The initial energy distribution for the surface conversion process is modeled according to results of numerical calculations by Eckstein et al. with the TRIM code [11]. Their results indicate that for low energies (3 eV) the angular distribution can be described by a cosine distribution. The acceleration within the plasma sheath depends on the potential difference, i.e. the difference of plasma potential and bias potential. The absolute value of the starting velocity of the surface generated negative ions is taken as an input parameter which can be adjusted in the experiment by varying the bias potential.
Strong electric fields are established between the plasma and extraction grid, forming spherically curved boundary surfaces, which repel positive ion plasma components. These surfaces are called plasma meniscuses or extraction surfaces. Negative ions

entering these interfacial surfaces are considered as extracted from the source plasma and the trajectory computation for the individual negative ion is stopped. To calculate the plasma meniscus, it is necessary to consider the influence of the ion beams space charge on the electric field. Therefore, the self consistent Ray Tracing code KOBRA3 [12] was used to calculate the shape of the plasma meniscus for typical conditions of the RF-driven ion source.
Negative ions redirected towards the extraction system can either reach an aperture of the plasma grid or enter the sheath, where a specular reflection results in a re-entering into the plasma volume.
A statistics of extracted and destroyed ions for a large ensemble of pseudo particles is calculated for starting coordinates, which are homogeneously distributed over the converter surface. Surface densities up to 10^5 particles for a surface cell of 1 mm^2 area were used in the simulation. These densities are necessary to achieve a statistics which is sufficient for a spatial resolutions of the extraction probability and the current density.

4.2. Computational Methods

The transport simulation is based on the solution of ordinary differential equations in a constant 3D electric $E(x, y, z)$ and magnetic $B(x, y, z)$ field topology for a statistical significant number of initial conditions. These initial conditions were determined by a Monte Carlo algorithm using a normal distribution of the spatial coordinates on the converter surface and a cosine distribution with respect to the surface normal vector of the initial velocity vector. The modified Lorentz equation

$$m\,\ddot{\vec{r}} = q\,(\vec{E} + \vec{v} \times \vec{B}) + \vec{F}_{\mathrm{Col}}, \tag{1}$$

is solved in succession for independent test particles by a combination of a Runge Kutta method and a Monte Carlo method to treat the collision force term $\vec{F}_{\mathrm{Col}}$. The electric $E(x, y, z)$ and magnetic field $B(x, y, z)$ are calculated by a linear interpolation scheme for given field maps. At each time step Δt, the particle position and velocity vector calculated by the Runge Kutta method [13] are altered by elastic and inelastic collisions. Elastic coulomb collisions with H^+ plasma particles are taken into account every time step. These are treated by a binary collision model [14]. The probability P_{Col} of an inelastic collision is calculated by the path length estimator algorithm according to

$$P_{\mathrm{Col}} = 1 - \mathrm{e}^{-\Delta t \sum\limits_j \nu_j}, \tag{2}$$

where ν_j is the collision frequency of an inelastic collisions of type j. If an inelastic collision takes place, one of the processes is chosen randomly according to the individual collision probability. This probability is calculated as follows:

$$P_j = \frac{n_j\, X_j}{\sum\limits_i n_i\, X_i}, \tag{3}$$

where n_j is the density of species j and $X_j =< \sigma_j v >_{\mathrm{Maxwell}}$ the rate coefficient for the j-th process [15]. This coefficient is obtained by an integration of the product of relative

velocity and collision cross section σ_j for a Maxwellian velocity distribution.
Two different types of inelastic collisions were considered in the transport code: destructive and non-destructive collisions. If a destructive collision takes place, the H^- ion is lost by the collision process and the trajectory computation is stopped. The negative ion is conserved after the collision in case of a non-destructive collision and the trajectory computation is continued with an altered negative ion velocity vector. The post-collisional negative ion velocity is determined by a Monte Carlo algorithm depending on the properties of the collision partner.

4.3. Input Plasma Parameters

The calculation of the reaction rates requires the knowledge of particle densities and temperatures. Table 1 gives an overview of the plasma parameter used in the transport code. All plasma parameters were taken from experimental data described in [8].

Table 1. Particle densities and temperatures used in the code.

n_e	Electron Density	$5.5 \cdot 10^{17}\ m^{-3}$
T_e	Electron Temperature	2.0 eV
n_H	H Atom Density	$1.0 \cdot 10^{19}\ m^{-3}$
T_H	H Atom Temperature	0.8 eV
n_{H_2}	H_2 Density	$4.0 \cdot 10^{19}\ m^{-3}$
T_{H_2}	H_2 Temperature	1200 K
H^+	H^+ Ion Density	$5.0 \cdot 10^{17}\ m^{-3}$
T_{H^+}	H^+ Ion Temperature	0.8 eV
n_{Cs^+}	Cs^+ Ion Density	$5.0 \cdot 10^{16}\ m^{-3}$

The reaction probabilities were determined on basis of the rate coefficients and particle densities for the plasma parameters of the RF-driven ion source. Reactions with a negligible low reaction probabilities were omitted. Table 2 gives an overview of the reactions, which have significant influence on the Monte Carlo simulation.

Table 2. Processes taken account in the transport simulation.

Destructive		
Electron Stripping	$H^- + e \rightarrow H + 2e$	[16]
Mutual Neutralization	$H^- + H^+ \rightarrow 2H$	[17]
	$H^- + Cs^+ \rightarrow H + Cs$	[18]
Collisional Detachment	$H^- + H \rightarrow H + H + e$	[16]
	$H^- + H_2 \rightarrow H + H_2 + e$	[19]
Associative Detachment	$H^- + H \rightarrow H_2 + e$	[16]
Non-Destructive		
Charge Exchange	$H^- + H \rightarrow H + H^-$	[20]

5. Simulation of the LAG Extraction System

5.1. Trajectory Analysis

The transport simulation was used to investigate the LAG (Large Area Grid) extraction system [4], which is most commonly used in the experiments at the IPP. This system relies on extraction apertures with 8 mm diameter and 45° chamfered collars for negative ion extraction. The calculation domain was chosen to simulate the complete extraction system, which consists of two separate arrays of periodic arranged aperture rows with 146 apertures in total. Figures 4 and 5 show trajectories of extracted ions which were started in the middle of the upper half of the LAG extraction system. The calculated ion trajectories have typical path lengths of several centimeters depending on the starting position on the converter surface. Two distinct types of extracted ions were observed in the calculation. Directly extracted ions have short trajectories and enter the plasma interface after their generation on the chamfered aperture collar as shown in figure 4. The generation of directly extracted ions is assisted by an advantageous initial angle of the ion velocity vector with respect to the plasma meniscus. This velocity vector is constantly altered during the transport by collisions with the plasma particles and by the influence of magnetic field lines. Inelastic charge exchange collisions are of particular importance for this process. These collisions result in a direction change of the ion velocity vector, which is beneficial to redirection.

If the ion trajectory vector is disadvantageous for direct extraction, the ion trajectory length increases and the extraction takes place at the surrounding apertures. The extraction process is enhanced by the field lines of the long range filter field. Figure 5 shows trajectories of extracted ions with typical path lengths of several cm. Distortions by frequent Coulomb and efficient charge exchange collisions prevent the negative ions from a complete magnetization.

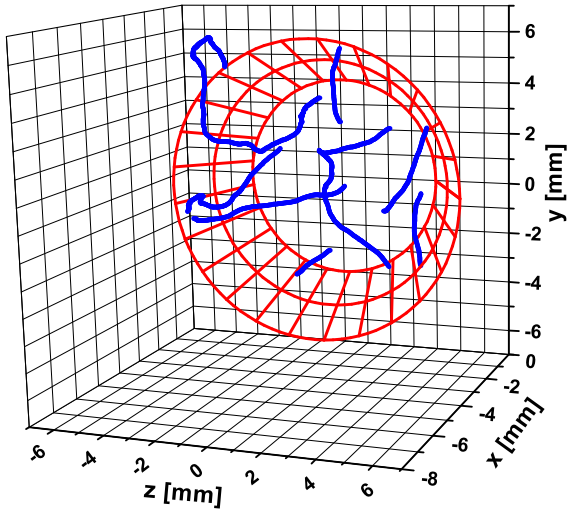

Figure 4. Trajectory plot of ions which were redirected immediate after their creation on the collar on a central aperture of the LAG extraction system for 1 eV starting energy.

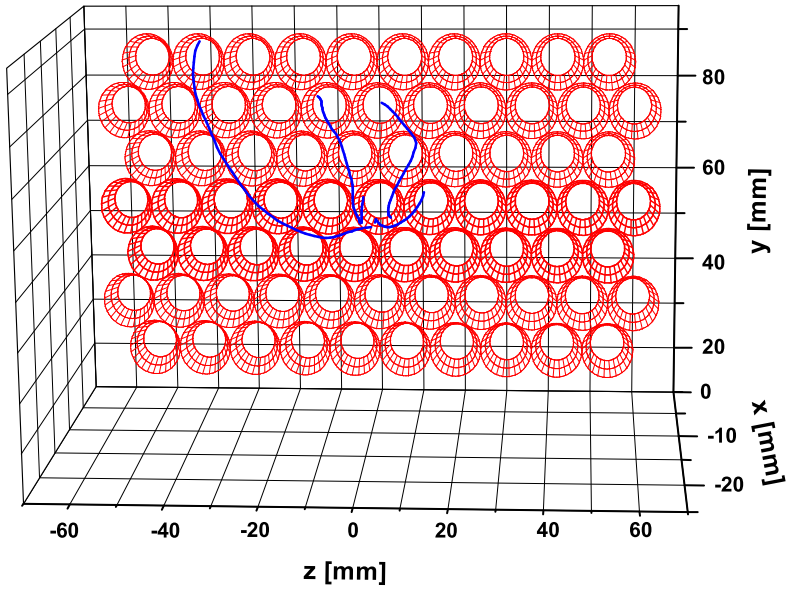

Figure 5. Trajectory plot of extracted ions which are gyrating around the magnetic filter field lines (z-direction) of the LAG system for a starting energy of 1 eV.

5.2. Integrated Extraction Probability

The quantity extraction probability is introduced in order to evaluate the quality of an extraction system. The local extraction probability $P_{\mathrm{loc}}(x, y)$ is defined as the number of extracted ions originating from an area element dA on the converter surface at position (x, y), divided by the number of ions generated on this element. The total or integrated

extraction probability is calculated by the surface integral

$$P_{\text{ext}} = \int_S P_{\text{loc}} dA, \tag{4}$$

taken over the converter surface.

The initial condition of the velocity vector is an important quantity for the transport of surface generated negative ions. The distribution of the ion starting vectors is influenced by the converter shape. Therefore, differently shaped converter surfaces were investigated. Besides the chamfered apertures, which are currently used for the LAG system, a configuration with a flat converter surface was investigated by means of the transport simulation. This flat configuration was used in earlier extraction experiments. Figure 6 shows the dependence of the extraction probability on the absolute value of the starting energy for the two converter configurations. The converter configuration with the chamfered collar area generates negative ions with a considerably higher extraction probability compared to the flat converter surface. The inclination of the vector of the initial velocity is very beneficial to the redirection process and allows a more efficient ion transport. The advantageous effect of chamfered collars on the extracted ion current is in in accordance with experimental observations [4].

Furthermore, the calculation shows that the extraction probability strongly depends on the initial energy of the surface generated negative ions. This initial energy is determined by the potential difference $\Delta\Phi$ between bias and plasma potential at the production surface. With decreasing $\Delta\Phi$, an increasing amount of ions can be extracted. This effect is especially pronounced for low starting energies (< 3 eV). The low starting velocity results in a higher retention time of the surface generated negative ions near the plasma grid. This enhances drastically the probability of an elastic collision, which will alter the original direction (into the plasma) near the apertures.

In addition, the effect of different ion velocities has an impact on the radius of ion gyration, which is influenced by the ion velocity and also by the magnetic field.

In order to determine the effect of the filter field on the extraction probability, the field strength was varied in the simulation, which corresponds to an enhancement or reduction of the permanent magnets in the filter boxes. For this investigation the filter field is characterized by the field strength of the filter field at the central position of the plasma grid. Figure 7 shows the dependence of the integrated extraction probability on the filter field strength (1 - 16 mT) for various initial energies (1,3,5,7 and 9 eV) of the negative ions. An extraction probability of up to 23 % is reached for the standard field strength of 7 mT. An increase of the filter field affects therefore primarily ions on long ranging trajectories. Both, a stronger magnetic field and a lower starting velocity, result in a reduction of the (effective) radius of ion gyration. This has an advantageous effect on the efficiency of ion transport: a smaller path length of the ion trajectories in the source plasma leads to a decrease of the probability of a destructive collision, therefore higher extraction probabilities are possible. Furthermore, a saturation of the extraction probability in case of starting energies above 7 eV was calculated for various filter field strengths. In case of high starting energies, a considerable amount of negative

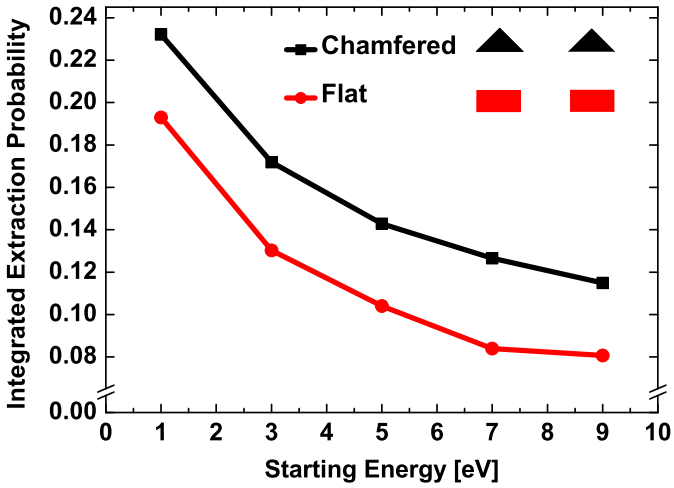

Figure 6. Calculated extraction probabilities of negative ions for the LAG extraction system for chamfered and flat converter shapes versus the ion starting energy (7 mT filter strength).

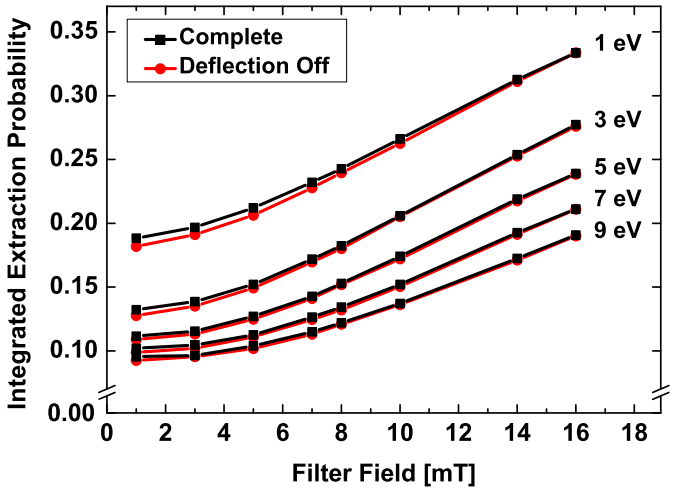

Figure 7. Calculated extraction probabilities of negative ions for the LAG extraction system versus the strength of the magnetic filter field for various ion starting energies and for two configurations of the magnetic field.

ions is lost by destructive collisions due to the increased radius of ion gyration. The remaining amount of extracted negative ions originates from the distribution of the ion starting velocity vectors causing a significant amount of ions, which are extracted due to an advantageous starting angle.

Filter and deflection field are treated separately in the code in order to allow variations of the individual fields. The effect of the electron deflection field on the ion transport is shown in figure 7. A calculation with deactivated deflection field for identical parameters

was done. It turned out, that the influence of the deflection field on the total amount of transported negative ions is negligible. Because of its short range, the deflection field does not contribute significantly to the amount of redirected ions.
Nevertheless, changes of the magnetic field and potential difference affect the plasma particle fluxes and therefore the surface density of generated negative ions, which was kept constant for the transport simulation. Correlations with experimental observation require therefore a plasma model to consider the altered wall fluxes.

5.3. Spatial Resolution

Besides the calculation of the integrated transport quantities, the TrajAn code is also capable calculating the spatially resolved extraction probability and current density. Figure 8 shows a contour plot of the local extraction probability on the plasma grid converter for 1 eV starting energy and the standard magnetic field configuration. The profile shows, that the local extraction probability has a maximum at the chamfered area. The inclined starting vectors on the collar area segments lead to trajectories with a higher redirection probability. On the one hand, an ion velocity vector with a parallel component is beneficial to its bending towards the plasma grid; on the other hand, trajectories with inclined starting angles are in closer proximity to the plasma interface increasing the probability of an extraction.
However, at the peripheral areas of the aperture array, the extraction probability is drastically reduced to values below 15 %. Apart from the aperture collars, the extraction probability is limited because of the spatial distance to the aperture area.

The profile of the extraction probability on the aperture collars is affected by the orientation of the local magnetic field vector. This vector results from a superposition of the filter field in z-direction and the deflection field, which alternates in y-direction. This yields a shift in y-direction, alternating in positive and negative z-direction depending on the magnetization of the individual magnet row pair. The deflection field predominantly influences the process of direct extraction. This causes a redistribution of the local extraction probability, while the integral value is unaffected.
An important quantity for the homogeneity of the ion beam, which is a superposition of the current densities of the individual apertures. This local current density is determined in the simulation by dividing the number of ions extracted through an element on the transparent aperture area by the area of this element. Figure 9 shows a contour plot of the current density over several apertures for a starting energy of 1 eV and the standard magnetic field configuration. The calculated current density profiles show an increases of 30-40 % toward the edge of the individual aperture area. In addition, the current density is shifted in a similar way as the extraction probability by the magnetic field configuration.

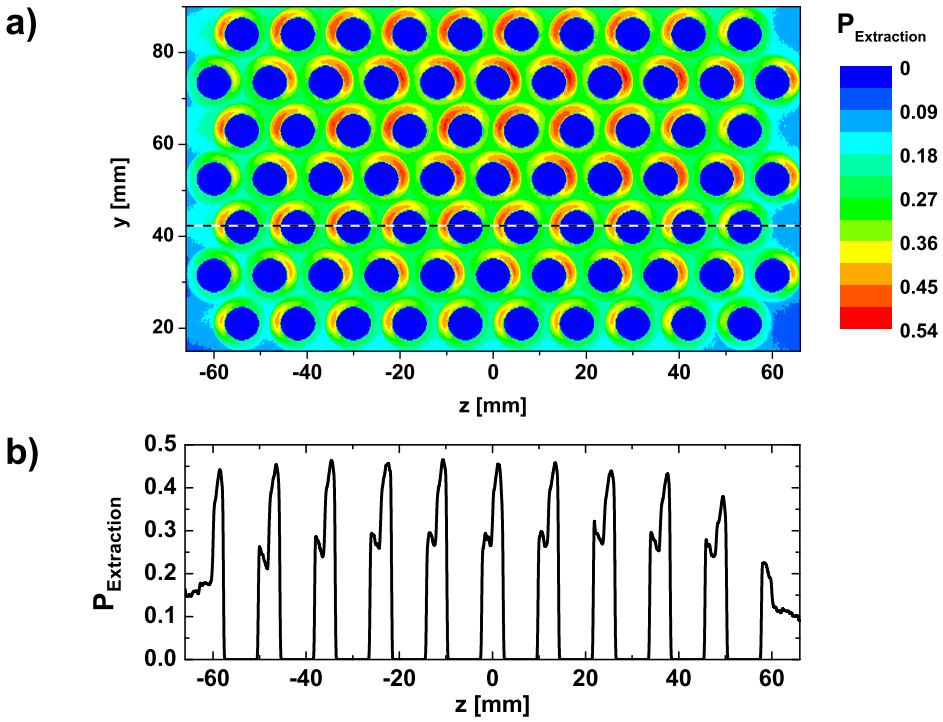

Figure 8. (a) Spatially resolved extraction probability for the upper half of the LAG extraction system for the standard magnetic field configuration (7 mT) and 1 eV starting energy. (b) Extraction probability across the dashed line in figure (a).

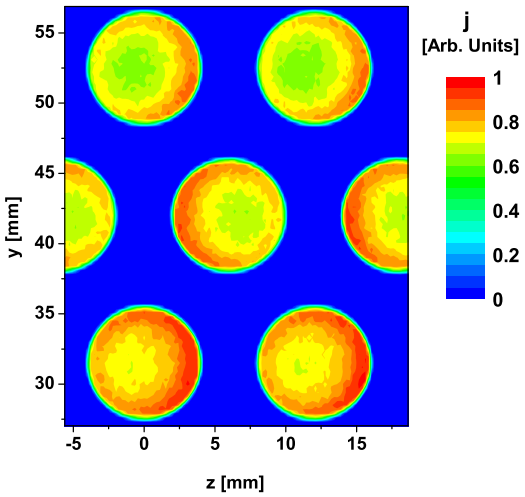

Figure 9. Spatially resolved current density for apertures from the upper half of the LAG extraction system for the standard magnetic field configuration (7 mT) and 1 eV starting energy.

6. Conclusion and Outlook

A probabilistic negative ion transport code for realistic field topologies and converter geometries was developed and applied to simulate the large scale extraction system LAG of the IPP RF-driven ion source. The advantageous effect of chamfered aperture collars on the extracted ion current, which was observed in the experiment, is cause by the modified distribution of the initial ion velocities.
An investigation of the ion dynamics showed a strong effect of the radius of ion gyration on the extraction probability. This probability can be increased by a reduction of the initial ion energy and by an increase of the filter field strength.
An analysis of the magnetic field revealed, that the total amount of extracted ions is not affected by the short ranging deflection field. Nevertheless, a study of the extraction probability profiles on the converter surface shows areas of intensified extraction probability depending on the local orientation of the magnetic field vector strongly influenced by the deflection field.
The calculation of the spatially resolved quantities within a large extraction system makes it possible to investigate the effect of different physical factors on the homogeneity of the ion beam, which can be achieved by using the calculated current density profiles as input parameters for ion optics simulations.

Acknowledgments

This work was (partly) supported by a grant from the European Union within the framework of EFDA (European Fusion Development Agreement). The authors are solely responsible for the content.

References

[1] K.H. Berkner, R. V. Pyle and J. W. Stearns, *Nucl. Fus.* **15** (1975), 249
[2] R. S. Hemsworth, A. Tanga and V. Antoni, *Rev. Sci. Inst.* **79** (2008), 02C109
[3] ITER Technical Basis 2002, ITER EDA Documentation Series No 24 (Plant Description Document, section 2.5.1), IAEA Vienna
[4] E. Speth, H. Falter, P. Franzen, U. Fantz et al, *Nucl. Fusion* **46** (2006), 220
[5] U. Fantz et al., *Plasma Phys. Control. Fusion* **49** (2007), B563B580
[6] O. Fukumasa and R. Nishida, *Nucl. Fusion* **46** (2006), 275
[7] D. Riz and J. Pamela, *AIP Conference Proceedings* **380** (1996), 3
[8] U. Fantz U et al, *Nucl. Fusion* **46** (2006), S297
[9] W. G. Graham, "Properties of Alkali Metals Adsorbed onto Metal Surfaces" in Proc. 10th Symp. on Fus. Tech., Brookhaven National Laboratory, Upton, 1980
[10] M. Seidl et al, *J. Appl. Phys.* **79** (1996), 6
[11] W. Eckstein et al, *Appl. Phys.* **A38** (1985), 123
[12] P. Spädtke and S. Wipf, *GSI Report* **89-09** (1989)
[13] W. Press, S. Teukolsky, W. Vetterling and B. Flannery, "Numerical Recipes in Fortran 90: The Art of Parallel Scientific Computing 2nd edn", Cambridge University Press, Cambridge, 1996
[14] S. Ma, R. Sydora and J. Dawson, *Comp. Phys. Comm.* **77** (1993), 190

[15] C. Birdsall, *IEEE Trans. on Plasma Sci.* **19**, 1991, 65
[16] R. Janev, W. Langer, J. Evans and D. Post, "Elementary Processes in Hydrogen-Helium Plasmas", Springer, Berlin, 1987
[17] M. Eeerden, M. van Sanden, D. Otorbaev and D. Schram, *Phys. Rev. A* **51** (1994), 3362
[18] R. Janev and Z. Radulovic, *Phys. Rev. A* **17** (1978), 889
[19] C. F. Barnett, Oak Ridge National Laboratory, Technical Report ORNL-6086, 1990.
[20] M. Huels, R. Champion, L. Doverspike and. Y. Wang, *Phys. Rev. A* **41** (1990), 4809